

# First-principles theory of magnetically induced ferroelectricity in $\text{TbMnO}_3$

Andrei Malashevich\* and David Vanderbilt

*Department of Physics & Astronomy, Rutgers University, Piscataway, NJ 08854-8019, USA*

(Dated: May 19, 2009)

We study the polarization induced via spin-orbit interaction by a magnetic cycloidal order in orthorhombic  $\text{TbMnO}_3$  using first-principle methods. The case of magnetic spiral lying in the  $b$ - $c$  plane is analyzed, in which the pure electronic contribution to the polarization is shown to be small. We focus our attention on the lattice-mediated contribution, and study its dependence on the Coulomb interaction parameter  $U$  in the LDA+ $U$  method and on the wave-vector of the spin spiral. The role of the spin-orbit interaction on different sites is also analyzed.

PACS numbers: 75.80.+q, 77.80.-e

## INTRODUCTION

Magnetically induced ferroelectricity provides a route to materials with a large magneto-electric (ME) coupling. The appearance of the ferroelectric order simultaneously with the onset of a particular magnetic order suggests that the magnetic and electrical properties should be strongly interconnected. Therefore, one might expect to observe a strong dependence of the electric polarization on external magnetic fields in such materials. Indeed, a pronounced interplay between ferroelectricity and magnetism was observed experimentally [1, 2, 3, 4] in  $(\text{Gd,Tb,Dy})\text{MnO}_3$ ,  $(\text{Tb,Dy})\text{Mn}_2\text{O}_5$ ,  $\text{Ni}_3\text{V}_2\text{O}_8$ , etc. In these materials, ferroelectricity is induced by a specific (e.g., cycloidal) magnetic ordering. Since polarization is a polar vector quantity, it is necessary to break the inversion symmetry in order for the ferroelectric phase to appear. In magnetically induced ferroelectrics, the inversion symmetry can be broken by the magnetic order alone, or in some cases, by the magnetic order in combination with the crystal structure (e.g., in  $\text{Ca}_3\text{CoMnO}_6$  [5]), where separately both the lattice and magnetic structures have inversion symmetry. The spin-orbit (SO) coupling is essential in order to allow the broken symmetry to be communicated from the magnetic to the charge and lattice degrees of freedom.

In our work, we focus our attention on  $\text{TbMnO}_3$ , in which the appearance of polarization is attributed to the cycloidal order of magnetic moments on the  $\text{Mn}^{3+}$  sites.  $\text{TbMnO}_3$  is an orthorhombically distorted perovskite material whose lattice has  $Pbnm$  symmetry with 20 atoms per unit cell. The magnetic properties of  $\text{TbMnO}_3$  are mainly due to the  $\text{Mn}^{3+}$  ions. The competition between the nearest-neighbor and next-nearest-neighbor spin interactions leads to a rich phase diagram. Experimentally it is known that below  $\sim 41$  K the magnetic moments form a sinusoidally modulated antiferromagnetic order. Below  $\sim 27$  K, a phase transition occurs in which the magnetic order develops a cycloidal character (with spins in the  $b$ - $c$  plane) with modulation wave-vector  $k_s \sim 0.28$  along  $b$ , and a polarization simultaneously appears along  $c$ . Phenomenological and microscopic theoretical mod-

els [6, 7, 8] can explain how the cycloidal magnetic order can drive the system to become ferroelectric, and one can predict the direction of the polarization (but not its sign) on rather general symmetry grounds. However, it is unclear whether one should expect the ionic displacements (phonons) to play the most significant role in creating electric polarization, or whether a purely electronic mechanism could explain the observations.

Our previously-reported initial findings [18] and a related study [19] suggested that, at least in the case of the spin spiral lying in the  $b$ - $c$  plane, the lattice contribution to the polarization dominates over the electronic contribution in  $\text{TbMnO}_3$ . However, these works left several questions unanswered. Here, we first briefly review our earlier work, emphasizing a careful analysis of the lattice-mediated contribution to the polarization using first-principles calculations. We then discuss several extensions of the work, including a study of the dependence of the results on the choice of  $U$  parameter, additional details concerning the site-specific spin-orbit interaction and its effects on the dynamical effective charges, and a more thorough and revealing investigation of the dependence of the polarization on the wave-vector of the spin spiral.

## COMPUTATIONAL DETAILS

The electronic-structure calculations are based on the density functional theory (DFT) and are performed using the projector-augmented wave (PAW) method [10, 11] in a plane-wave basis set. The plane-wave energy cutoff is 500 eV. We use the VASP code package [9] for our calculations. We do not include  $f$  electrons in the Tb PAW potential. The local-density approximation for the exchange-correlation functional is used (Ceperley-Alder [12] with Vosko-Wilk-Nusair correlation [13]). For a proper treatment of Mn  $d$  electrons, we use on-site Coulomb corrections implemented in a rotationally-invariant LDA+ $U$  formulation [14]. We consider two values of  $U$ , 1 and 4 eV. The results of a systematic study with  $U = 1$  eV were reported previously in Ref. [18];

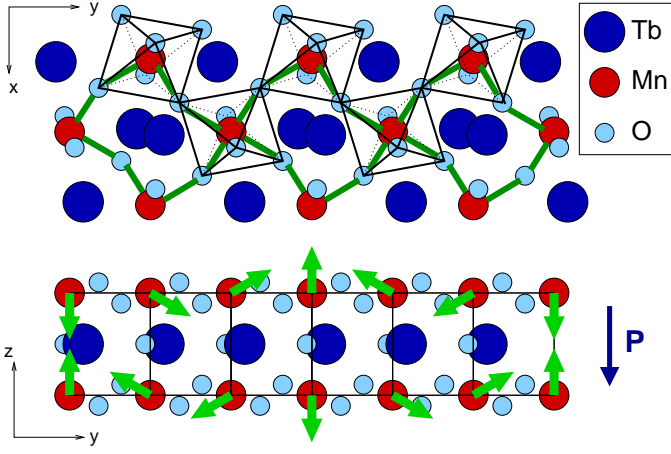


FIG. 1: Sketch of the  $a \times 3b \times c/2$  orthorhombic cell of  $\text{TbMnO}_3$  ( $Pbnm$  space group) showing  $\text{MnO}_6$  octahedral tilts (top) and the cycloidal magnetic structure on the  $\text{Mn}^{3+}$  sites (bottom).

some of these will be reproduced here for comparison. We consider the cycloidal magnetic order having a spin spiral lying in the  $b$ - $c$  plane and wave-vector  $k_s$  propagating in the  $b$ -direction (see Fig. 1). The experimental value of the wave vector is incommensurate with the lattice,  $k_s \sim 0.28$  [1]. Since we use periodic boundary conditions, we study commensurate cycloidal spin structures with wave-vectors  $k_s = 0, 1/4, 1/3, 1/2, 2/3$  and 1 using appropriate supercells. The structural relaxation was performed with  $k_s = 1/3$  (60 atoms per cell), which is close to the experimental  $k_s$  (Fig. 1). A  $3 \times 1 \times 2$   $k$ -point sampling is used. The Berry-phase approach [16] is used for the calculation of the electric polarization.

## RESULTS

### Dependence on $U$ parameter

A crystal structure optimization was performed for the 60-atom supercell using  $U = 1 \text{ eV}$  and  $U = 4 \text{ eV}$ . These calculations were carried out without SO interaction to obtain centrosymmetric reference structures, with respect to which Berry phase polarization will be calculated in the subsequent analysis. The lattice parameters and Wyckoff coordinates of the relaxed structures are given in Table I. For both values of  $U$ , the calculated structural parameters are very close to the experimental ones, with the lattice vectors being in slightly better agreement with experiment for the case of  $U = 4 \text{ eV}$ .

The calculation of the polarization in the presence of the SO interaction for these relaxed structures yields an estimate for the pure electronic contribution to the polarization. We find  $P^{\text{elec}} = 32 \mu\text{C}/\text{m}^2$  and  $P^{\text{elec}} = -14 \mu\text{C}/\text{m}^2$  for  $U = 1 \text{ eV}$  and  $U = 4 \text{ eV}$  respectively

TABLE I: Experimental (Ref. [17]) and theoretical ( $U=1 \text{ eV}$  is taken from Ref. [18]) structural parameters for orthorhombic  $\text{TbMnO}_3$ .

		Exp.	$U = 1 \text{ eV}$	$U = 4 \text{ eV}$
Lattice vectors	$a$ (Å)	5.293	5.195	5.228
	$b$ (Å)	5.838	5.758	5.775
	$c$ (Å)	7.403	7.308	7.343
Tb $4c(x y 1/4)$	$x$	0.983	0.979	0.980
	$y$	0.082	0.084	0.084
Mn $4b(1/2 0 0)$				
O1 $4c(x y 1/4)$	$x$	0.104	0.107	0.111
	$y$	0.467	0.469	0.465
O2 $8d(x y z)$	$x$	0.704	0.699	0.700
	$y$	0.326	0.320	0.323
	$z$	0.051	0.052	0.053

(with the direction of polarization parallel to the  $c$  axis, as was expected from symmetry). In both cases, the magnitude is much smaller than the observed value of  $\sim 600 \mu\text{C}/\text{m}^2$  [1], indicating that it can be neglected for any reasonable value of  $U$ .

To analyze thoroughly the role of the ionic displacements, we computed the Hellmann-Feynman forces which appeared on the ions after the SO interaction was turned on. Keeping in mind that only zone-center infra-red active modes can be responsible for the appearance of polarization, we filtered out the forces that did not act on these modes. We found that the infra-red active modes that were left had dynamical dipoles along  $c$  as expected. There are eight such modes: three associated with Mn atoms in Wyckoff position  $4b$ , one each for Tb and O1 atoms in Wyckoff position  $4c$ , and three for the O2 atoms in Wyckoff position  $8d$  [20]. To find the ionic displacements induced by the SO interaction, we used the force-constant matrix [18] calculated in the absence of SO using the 60-atom supercell. (We note however that one could have used the 20-atom unit cell for this calculation, with  $k_s = 0$ , since the force-constant matrix depends only weakly on the wave-vector.) Updating the ionic positions according to the calculated displacements and carrying out Berry-phase polarization calculations for the resulting structures, we find the total polarization induced by the SO interaction. The results for  $U = 1 \text{ eV}$  and  $U = 4 \text{ eV}$  are  $P^{\text{tot}} = -467 \mu\text{C}/\text{m}^2$  and  $P^{\text{tot}} = -218 \mu\text{C}/\text{m}^2$  respectively. Knowing the ionic displacements, one can also find the contributions to the polarization from each mode by calculating the effective charges of the modes. The results of such calculations for both values of  $U$  are given together with the forces in Table II.

Note that the values for the forces in the second column of the table represent the forces acting on the ‘modes’ rather than ions themselves. Each mode is character-

TABLE II: Forces  $F$  (meV/Å), effective charges  $Z$  ( $e$ ), and contributions  $\Delta P$  to the polarization ( $\mu\text{C}/\text{m}^2$ ) from IR-active modes. See text for the description of the conventions used to describe the modes. The values for  $\Delta P^*$  are calculated with the SO coupling turned off everywhere except on Mn sites.

Wyckoff mode	$U = 1 \text{ eV}$				$U = 4 \text{ eV}$	
	$F$	$Z$	$\Delta P$	$\Delta P^*$	$F$	$\Delta P$
Tb 4c, $z$	0.43	7.47	-94	-73	0.47	-42
O1 4c, $z$	2.26	-6.82	81	69	1.46	15
Mn 4b, $x$	-7.04	0.57	-13	-14	-2.00	-3
Mn 4b, $z$	-8.93	7.46	-248	-232	-3.86	-94
Mn 4b, $y$	-2.94	0.55	0	-1	-1.06	2
O2 8d, $x$	5.06	0.08	3	2	2.00	2
O2 8d, $y$	3.57	0.23	16	9	1.59	6
O2 8d, $z$	4.41	-5.74	-234	-208	1.37	-87
			-489	-448		-201

ized by a unit vector in the  $(20 \times 3)$ -dimensional space. Therefore, to get the actual number for the force acting on a particular ion, one must multiply the corresponding value from the table by an appropriate unit vector. This procedure will give absolute values for the ionic forces that are two times smaller than the numbers in the table for the first five modes, and  $2\sqrt{2}$  times smaller for the rest of the modes.

The decomposition of the lattice-mediated polarization into mode contributions is discussed in detail in Ref. [18]. Here we compare the results obtained with different Coulomb interaction parameters. The results in Table II for  $U = 1 \text{ eV}$  and  $U = 4 \text{ eV}$  may seem different, but in fact they are qualitatively similar. The forces may be viewed as vectors in an 8-dimensional space, and one can calculate the angle  $\theta$  between them to find  $\cos \theta \sim 0.98$ . Thus, the direction of the forces is almost the same, although the magnitude is different. This means that the underlying physical mechanism of the magnetically induced polarization does not depend strongly on the choice of  $U$ , while the magnitude of the effect does change with  $U$ .

In the subsequent sections we will consider only  $U = 1 \text{ eV}$ , which gives better agreement with the experimental polarization. Moreover, in this case the calculated band gap matches the experimental value of  $\sim 0.5 \text{ eV}$  [15]. In general, a better strategy for choosing the  $U$  value would be to calculate the exchange parameters and fit those, rather than the band gap, to the experimental data. In the present case, however, such an approach leads to a similar choice [19] of parameters.

## Site-specific spin-orbit interactions

To better understand the role of the spin-orbit interaction, we studied how the behavior of the system changes depending on the strength of the SO interaction and on the presence of SO on various atomic sites. We performed calculations of the forces with the SO interaction turned off on all sites other than Tb, then Mn, then O. Using the force-constant matrix, we estimated the lattice contributions to the polarization and found them to be  $-11 \mu\text{C}/\text{m}^2$ ,  $-447 \mu\text{C}/\text{m}^2$  and  $-8 \mu\text{C}/\text{m}^2$ , respectively. This result shows that the SO interaction on the Mn sites is responsible for almost all of the lattice-mediated contribution to the polarization (see the column for  $\Delta P^*$  in the Table II). We also calculated the purely electronic contributions to the polarizations for these three cases. Interestingly, the electronic contribution comes almost entirely from the spin-orbit effect on the Tb sites. Several calculations of the forces with modified SO strength confirmed that they depend linearly on the SO strength.

## Dependence on wave-vector

Microscopic theoretical models involving the displacements of ions [8, 22, 23] show that the Dzyaloshinskii-Moriya (DM) interaction can induce ferroelectric displacements of ions. Usually, only the interaction between the nearest-neighbor transition metals is considered in such models. As a consequence, the polarization is expected to depend sinusoidally on the angle between the spins of the nearest-neighbor Mn sites,  $\mathbf{P} \propto \mathbf{e}_{n,n'} \times (\mathbf{S}_n \times \mathbf{S}_{n'})$  [24], and thus sinusoidally on  $k_s$ . To study the dependence of the lattice contribution to the electric polarization on  $k_s$ , we have carried calculations of the SO-induced forces for a 40-atom supercell ( $k_s=1/2$ ) and an 80-atom supercell ( $k_s=1/4$ ). Note also that the same 60-atom supercell can be used to set up a spiral with the wave-vector  $k_s=2/3$ . In general, if the supercell consists of  $n$  primitive cells, one can construct spirals with wave-vectors  $m/n$ , where  $0 \leq m \leq n$ . We also used the primitive 20-atom cell for the calculations with  $k_s = 0$  and  $k_s = 1$ . In all these calculations we kept the same structural coordinates as for the 60-atom structure to make sure that we only change one parameter ( $k_s$ ) in this study. We calculated the forces, and again filtered those that were IR-active. We find that the pattern of the IR forces matches almost exactly that of the 60-atom cell, i.e., the directions of the eight-dimensional vectors almost coincide in all cases. Using the force-constant matrix calculated on the 60-atom supercell and the effective charges from Table II, we can estimate the polarization for the new wave-vectors. The result is shown in Fig. 2. Actual calculations were performed only for non-negative values of  $k_s$ , as symmetry arguments show that polarization must be an odd function of spin-spiral wave-vector. The

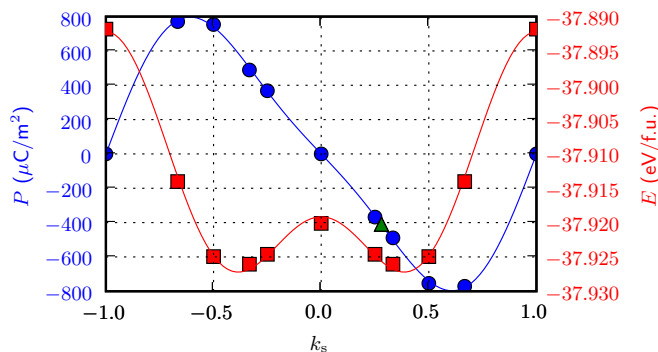


FIG. 2: Dependence of polarization (circles, scale at left) and total energy (squares, scale at right) on the spiral wave-vector  $k_s$ . The triangle indicates the extrapolation of the polarization to the experimental wave-vector of  $k_s = 0.28$ .

values  $k_s = 0$  and  $k_s = 1$  correspond to a collinear spin arrangement, in which cases the polarization was zero as expected. One can see that the dependence of the polarization on  $k_s$  deviates significantly from a simple sinusoidal form. Surprisingly, the polarization is almost linear in  $k_s$  up to  $k_s = 1/2$ ; such a linear dependence is expected in the long-wavelength limit, but that is a rather stretched assumption for  $k_s$  up to  $1/2$ . This result indicates that nearest-neighbor DM models oversimplify the mechanism of the polarization induction, and that taking the next-nearest-neighbor interactions into account may be important.

The experimental  $k_s$  lies in the range where we can assume a linear dependence. The extrapolation to  $k_s = 0.28$  yields a value for the lattice contribution of the polarization of about  $-410 \mu\text{C}/\text{m}^2$ . Fig. 1 also shows the dependence of the total energy per formula unit on the wave-vector. We remind the reader that in these calculations the structural parameters were kept fixed, with only the directions of the magnetic moments on Mn sites being changed. However, one can still see that the wave-vector at which the minimum occurs is close to the experimental value of  $k_s$ .

## SUMMARY

We have analyzed the lattice contribution to the electric polarization in the cycloidal-spin compound  $\text{TbMnO}_3$ , with the spin spiral lying in the  $b$ - $c$  plane, using

density functional theory within the LDA+ $U$  framework. We compare the results for two values of  $U$  (1 and 4 eV), and find that the mechanism of magnetoelectric coupling is quite independent of  $U$ . The dependence of the polarization on the spin-spiral wave period is studied in detail. We find that it deviates significantly from the sinusoidal dependence expected from simple models. The polarization is almost linear in wave-vector for absolute values of  $k_s$  up to 0.5.

This work was supported by NSF Grant No. DMR-0549198.

---

\* Electronic address: andreim@physics.rutgers.edu

- [1] T. Kimura *et al.*, Nature **426**, (2003) 55-58.
- [2] T. Lottermoser *et al.*, Nature (London) **430**, (2004) 541.
- [3] N. Hur *et al.*, Nature (London) **429**, (2004) 392.
- [4] G. Lawes *et al.*, Phys. Rev. Lett. **95**, (2005) 087205.
- [5] S.-W. Cheong and M. Mostovoy, Nat. Mater. **6**, (2007) 13.
- [6] M. Mostovoy, Phys. Rev. Lett. **96**, (2006) 067601.
- [7] H. Katsura, N. Nagaosa, and A. V. Balatsky, Phys. Rev. Lett. **95**, (2005) 057205.
- [8] I. A. Sergienko and E. Dagotto, Phys. Rev. B **73**, (2006) 094434.
- [9] G. Kresse and J. Furthmüller, Comput. Mater. Sci. **6**, (1996) 15; Phys. Rev. B **54**, (1996) 11169.
- [10] P. E. Blöchl, Phys. Rev. B **50**, (1994) 17953.
- [11] G. Kresse and D. Joubert, Phys. Rev. B **59**, (1999) 1758.
- [12] D. M. Ceperley and B. J. Alder, Phys. Rev. Lett. **45**, (1980) 566.
- [13] S. H. Vosko, L. Wilk, and M. Nusair, Can. J. Phys. **58**, (1980) 1200.
- [14] S. L. Dudarev *et al.*, Phys. Rev. B **57**, (1998) 1505.
- [15] Y. Cui, C. Wang, and B. Cao, Solid State Commun. **133**, (2005) 641-645.
- [16] R. D. King-Smith and D. Vanderbilt, Phys. Rev. B **47**, (1993) 1651.
- [17] J. A. Alonso *et al.*, Inorg. Chem. **39**, (2000) 917-923.
- [18] A. Malashevich and D. Vanderbilt, Phys. Rev. Lett. **101**, (2008) 037210.
- [19] H. J. Xiang and Su-Huai Wei and M.-H. Whangbo and Juarez L. F. Da Silva Phys. Rev. Lett. **101**, (2008) 037209.
- [20] E. Kroumova *et al.*, Phase Transit. **76**, (2003) 155-170.
- [21] Y. Yamasaki *et al.*, Phys. Rev. Lett. **98**, (2007) 147204; Phys. Rev. Lett. **100**, (2008) 219902(E).
- [22] A. B. Harris, J. Appl. Phys. **99**, (2006) 08E303.
- [23] C. D. Hu, Phys. Rev. B **77**, (2008) 174418.
- [24] T. Kimura, Annu. Rev. Matter. Res. **37**, (2007) 387-413.